Nuclear Engineering and Design 412 (2023) 112481

Contents lists available at ScienceDirect

Nuclear Engineering and Design

journal homepage: www.elsevier.com/locate/nucengdes

Experimental characterization of the flowline of a lithium film formed using an electromagnetic thruster for a RAON prototype charge stripper

Tae Uk Kang [a,1], Geunhyeong Lee [b,1], Hee Reyoung Kim [a,*]

[a] Ulsan National Institute of Science and Technology, Department of Nuclear Engineering, Ulsan 689-798, Republic of Korea
[b] Korea Atomic Energy Research Institute, 111, Daedeok-daero 989 beon-gil, Yuseong-gu, Daejeon 34057, Republic of Korea

ARTICLE INFO

Keywords:
Charge stripper
Electromagnetic thruster
Maintenance improvement
Liquid-lithium film

ABSTRACT

This paper describes the variable optimization of a lithium charge-stripper device for the Rare isotope Accelerator complex for ON-line experiences (RAON) and the experimental characterization of a lithium film formed for the charge removal of uranium using a magnetohydrodynamic liquid metal circulation system. To this end, liquid lithium charge stripper was fabricated to form a thin lithium film flow through collisions between a liquid lithium jet and a planar deflector. The flow characteristics of the lithium film were analyzed through simulation and waterjet experiments in terms of the liquid lithium film thickness. To circulate the liquid lithium, a mechanically safe electromagnetic thruster with precise pressure control was designed by analyzing its electromagnetic and hydraulic parameters through finite element simulation. The analysis of the geometrical arrangement of the permanent magnet and input current of the thruster revealed that compared to existing electromagnetic thrusters, the nominal input current of the newly-constructed thruster was reduced to 57% and its weight reduced to 6%, while facilitating easy maintenance. The optimized nozzle diameter and angle of the lithium charge stripper was 0.7 mm and 34°, respectively. Further, the formation of a 22-μm thick liquid lithium thin film required to obtain the 79^+ charge state of uranium was confirmed at an input current of 107 A.

1. Introduction

Rare isotope accelerator complex for ON-line experiments (RAON), which is Korea's first heavy ion accelerator, is being developed to accelerate the collision of heavy ions, such as uranium, with light element targets to obtain rare isotopes, and this requires charge removal and energy. Heavy ions are collided with light element targets using a device known as a charge stripper. To obtain a certain amount of uranium energy (200 Mev/u), the charge removal of heavy ions is essential. The charge stripper is commonly used to increase the charge state of a uranium beam with a charge state of 33^+ or 34^+ to 79^+ (Rare Isotope Science Project, 2012; Song, 2016). To achieve a mean charge state of 79^+, a liquid lithium thickness of 1.13×10^{-3} g/cm^2 (=22 μm) is required (Song, 2016). The efficiency of high-power heavy-ion accelerators can be enhanced using heavy-ion charge strips. To remove the charge from uranium, liquid lithium thin films, which exhibit a large operating temperature range (melting point of 181 °C, boiling point of 1342 °C), low vapor pressure (10^{-7} Pa at 200 °C) to minimize vapor pollution, low Prandtl number (~0.05), low thrusting power owing to its low density (513 kg/m^3), high heat capacity (4.4×10^{-3} J/kg • K), and low viscosity (Reed et al., 2016) has been applied. Liquid lithium thin films are formed by the jet spray of liquid lithium thrust from the jet nozzle of an electromagnetic thruster. As shown in Fig. 1, the flow of electrons from left to right in a liquid lithium thin film results in the removal of the electrons of the uranium beam, thus changing the charge state of uranium from 34^+ to 79^+ (Momozaki et al., 2009).

Owing to the high reactivity of liquid lithium with water and air, a non-contact electromagnetic thruster capable of generating electromagnetic force (Lorentz force) in liquid lithium is used for liquid lithium jet. Fig. 2 shows that the electromagnetic thruster is physically enveloped by the external environment without an internal structure, such as an impeller or a sealing part (Lee and Kim, 2018). However, the large weight (340 kg) of existing electromagnetic thrusters (Fig. 2) hinders their effective maintenance and management; therefore, this study redesigned the electromagnetic thruster to reduce its weight. The characteristics of the redesigned electromagnetic thruster are as follows. First, even if the magnetic field is not located in all directions (located only in one direction), there is no significant difference in the efficiency of the newly-designed thruster if the current only flows in the direction

* Corresponding author.
E-mail addresses: rkdxodnr25@unist.ac.kr (T.U. Kang), gh29@kaeri.re.kr (G. Lee), kimhr@unist.ac.kr (H.R. Kim).
[1] Lee and Kang contributed equally to this work.

https://doi.org/10.1016/j.nucengdes.2023.112481
Received 11 April 2023; Received in revised form 7 July 2023; Accepted 8 July 2023
Available online 12 July 2023

Nomenclatures

$\vec{B}$	Magnetic flux density [T]
B_t	Time-varying magnetic flux density [T]
B_r	r- direction magnetic flux density [A/m^2]
B_θ	θ – direction magnetic flux density [A/m^2]
B_z	z – direction magnetic flux density [A/m^2]
D	Hydraulic diameter [m]
d	Diameter [m]
E	Electric field [V/m]
E_t	Time-varying electric field [V/m]
E_p	electromotive force [n]
f	Force [N]
f_r	Friction factor
f_d	friction coefficient
f_d	Darcy friction coefficient of turbulent flow
H	Magnetic field intensity [A/m]
H_d	Height of the duct [m]
H_m	Magnetic field intensity of the permanent magnet [A/m]
i_{ver}	Current flowing [A]
i_p	Input current [A]
i_f	Fringing resistance [Ω]
J	Current density [A/m^2]
J_r	r- direction current density [A/m^2]
J_θ	θ - direction current density [A/m^2]
J_z	z – direction current density [A/m^2]
K_B	Total bend coefficient
K_1	Band resistance coefficient
L	Total length [m]
M	Magnetization [A/m]
n	Number of duct turns
R_f	Fringing resistance [Ω]
R_s	Resistance vertical to the current [Ω]
R_o	Outer resistance [Ω]
R_p	MHD circulator resistance [Ω]
R_{ver}	Vertical component resistance [Ω]
Re	Reynolds number
r	Duct radius (m)
t	Time [s]
v	Velocity [m/s]
W_d	Width [m]
ε_0	Electrical permittivity in vacuum [$=8.85 \times 10^{-12}$ F/m]
ε_s	roughness height
ρ	Density [kg/m^3]
Δp_h	Hydraulic pressure loss [bar]
σ	Electrical conductivity [S/m]
μ_0	Magnetic permeability in vacuum [$=4\pi \times 10^{-7}$ H/m]
μ_r	Relative magnetic permeability
χ_m	Magnetic susceptibility

where the magnetic field is applied. By attaching a magnet to one direction of the duct, the magnetic field strength increases and the amount of ferromagnetic material required to shield the magnetic field reduces considerably, enabling the circulation of a small amount of liquid lithium. In addition, the redesigned structure increased the convenience of the maintenance process as the flow path can be easily replaced. A direct current (DC) conduction-type electromagnetic thruster requires a high current but less voltage (<1 V); thus, even if the resistance of the electrode is large, copper corrosion can be prevented by replacing copper with stainless steel (SUS316). Accordingly, the electromagnetic thruster coil and charge stripper system of the newly designed thruster were composed of SUS316, which is a non-reactive material in a lithium fluid flow environment (an alkali metal), enabling continual stable operation. The operating temperature and pressure of the lithium charge stripper for RAON are 200 ℃ and 10^{-7} Pa, respectively. The injection velocity of the lithium flow, which is achieved using an electromagnetic thruster, from the nozzle of the charge stripper system and the thickness (22 μm) of the lithium film are required (Song, 2016). In this study, a DC conduction helical-type magnetohydrodynamic (MHD) electromagnetic thruster, which significantly decreased the required input power by minimizing the input current, was newly designed and constructed to circulate a continuous liquid lithium film flow for a charge stripper prototype that would be used in RAON. The prototype of the charge stripper for RAON was manufactured for the formation of lithium films,

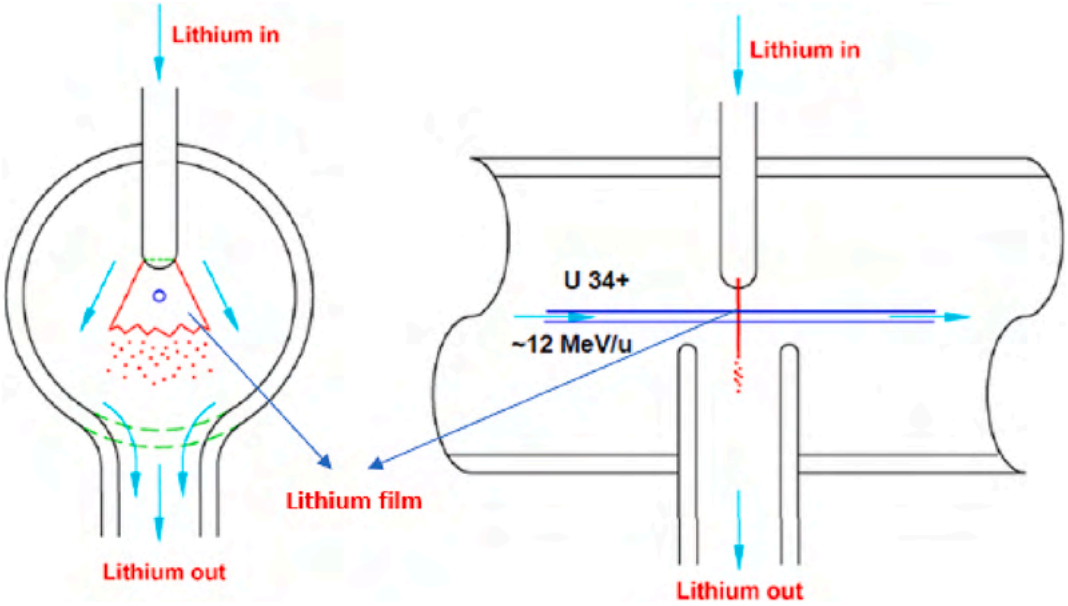

Fig. 1. Charge removal process of a uranium ion passing through a liquid lithium film.

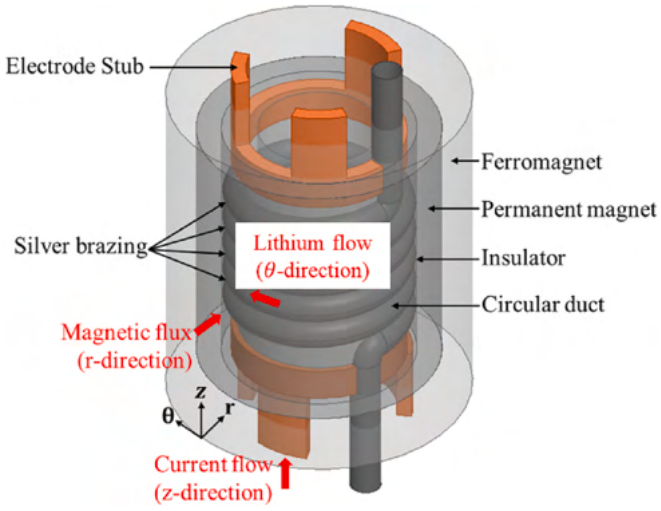

Fig. 2. Design concept of the helical-type electromagnetic thruster.

where liquid lithium was circulated to the charge stripper prototype through the electromagnetic thruster, and the characteristics of the liquid lithium film were analyzed.

2. Methods

2.1. Theoretical approach for the design analysis of the helical-type electromagnetic thruster

The design variables were determined by solving MHD equations, including the electromagnetic and fluid equations. Ampere's law, Faraday's law, Gauss' law for magnetism, Ohm's law, and the fluid equation are expressed in Eqs. (1)–(4).

$$\text{Ampere's law}: \nabla \times \vec{B} = \mu_0\left(\vec{J} + \varepsilon_0\frac{\partial E}{\partial t}\right), \tag{1}$$

$$\text{Faraday's law}: \nabla \times \vec{E} = -\frac{\partial \vec{B}}{\partial t}, \tag{2}$$

$$\text{Gauss's law for magnetism}: \nabla \bullet \vec{B} = 0, \tag{3}$$

$$\text{Ohm's law}: \vec{J} = \sigma\left(\vec{E} + \vec{v} \times \vec{B}\right). \tag{4}$$

The magnetic field was simulated using ANSYS Maxwell. The boundary conditions were identical to those presented in Eqs. (5)–(9). The magnetic flux density in the flow path was analyzed using the finite element method (FEM) by applying the coercive force of a permanent magnet and the permeability of the ferromagnetic material. Magnetization (M) can be expressed as a relationship between the magnetic field strength (H) of the ferromagnetic material and the magnetic field strength of a permanent magnet (H_m) by considering both the permanent magnet and ferromagnetic material. This relationship can be expressed using Eq. (5):

$$\vec{M} = \chi_m \vec{H} + \vec{H}_m \tag{5}$$

The overall magnetic flux density of the helical-type MHD electromagnetic thruster was calculated using Eq. (6), which considered the permanent and independent local magnetic fields, as well as the relative permeability:

$$\vec{B} = \mu_0\left(\vec{H} + \vec{M}\right) = \mu_0\mu_r\vec{H} + \mu_0\vec{H}_m \tag{6}$$

The boundary conditions between the magnetic field intensity and magnetic flux density of materials of different permeabilities were determined using Eqs. (7)–(9):

$$\vec{H}_{t,1} = \vec{H}_{t,2} \tag{7}$$

$$\vec{B}_{n,1} = \vec{B}_{n,2} \tag{8}$$

$$\vec{H}_t\Big|_{r=\infty} = 0 \tag{9}$$

This was simulated in COMSOL Multiphysics, and Eqs. (10)–(13) were used for the simulation. The force generated by the electromagnetic phenomenon was applied to the flow, and solved through coupling:

$$\vec{J}_t = \sigma\left(\vec{E}_t + \vec{v} \times \vec{B}_t\right) \tag{10}$$

$$\vec{J}_t = J_r\hat{r} + J_\theta\hat{\theta} + J_z\hat{z} \tag{11}$$

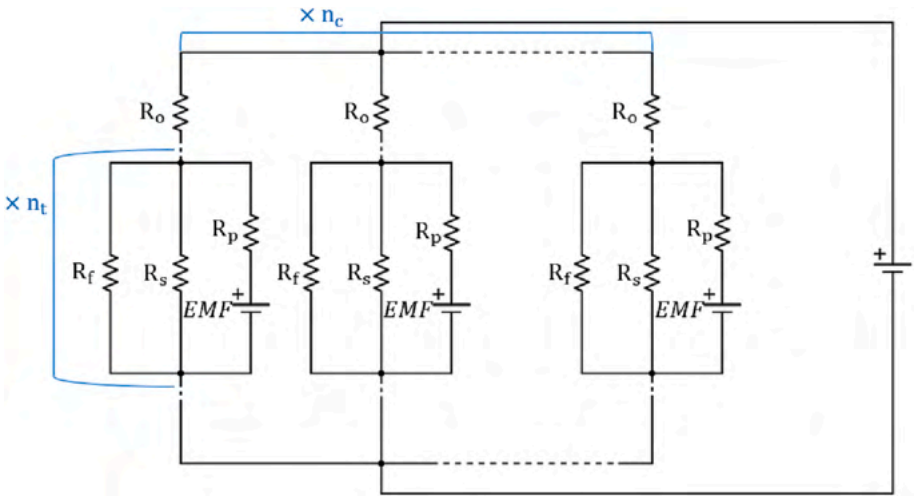

Fig. 3. Equivalent circuit of a helical-type magnetohydrodynamic (MHD) circulator.

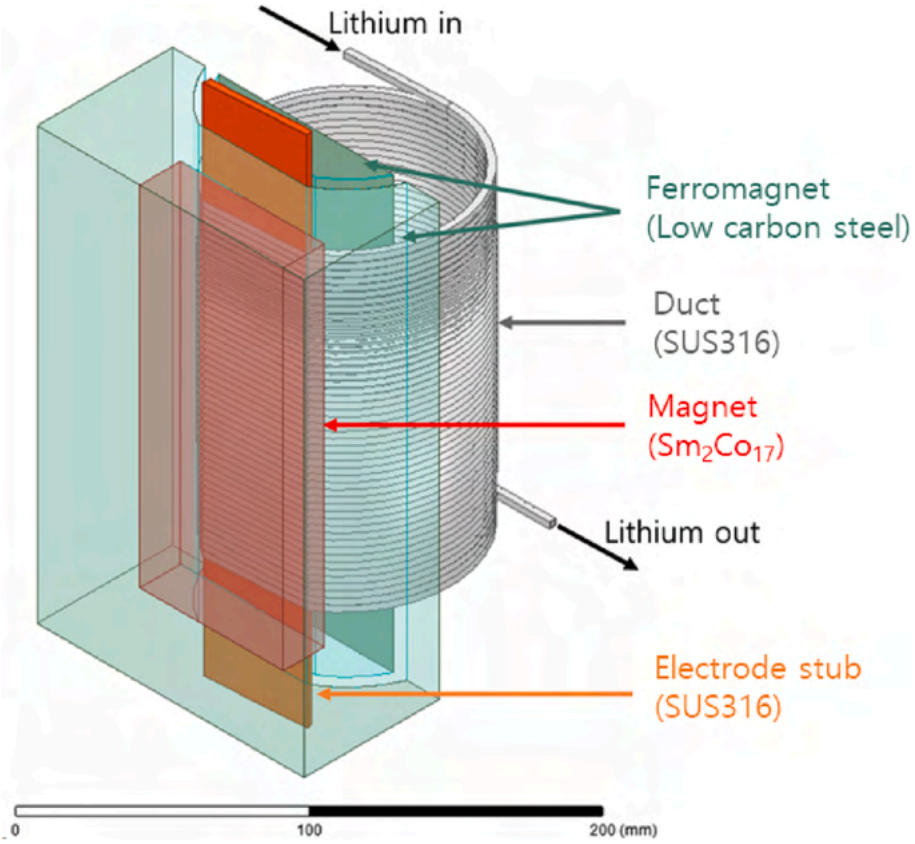

Fig. 4. Conceptual design of the helical-type electromagnetic thruster.

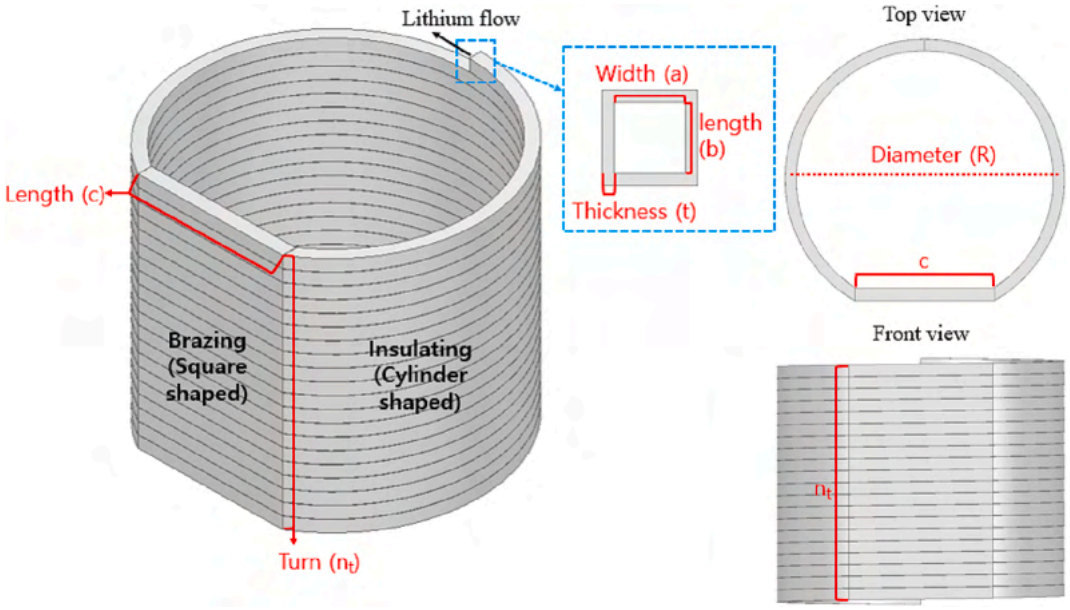

Fig. 5. Geometry of the electromagnetic thruster used for the simulation.

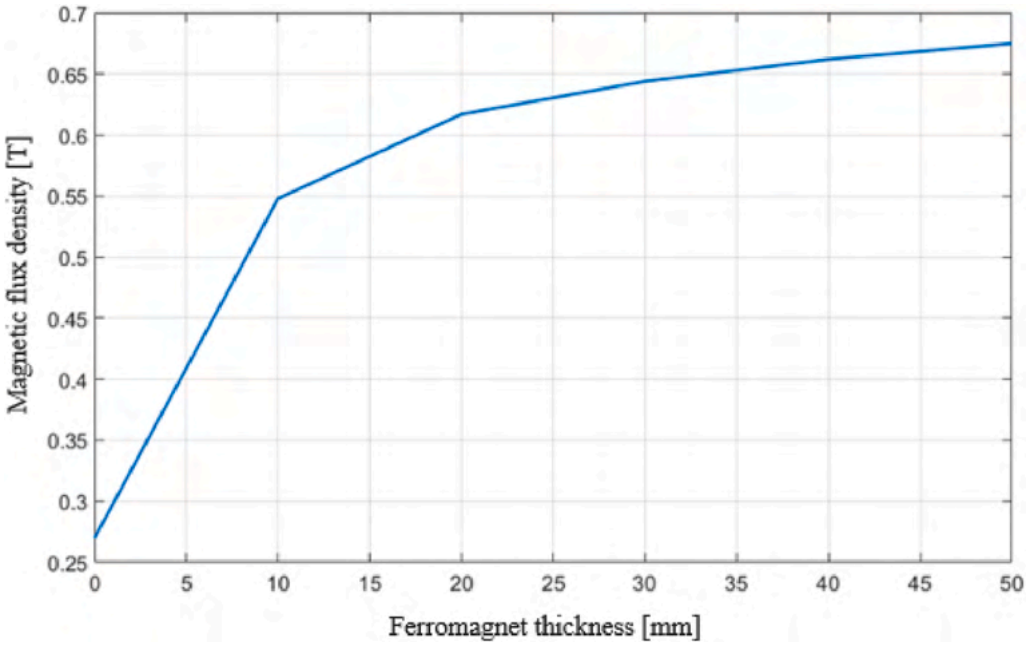

Fig. 6. Magnetic flux density according to the thickness of the ferromagnet (width = 5 mm, height = 5 mm, thickness = 0.5 mm, and number of turns = 30).

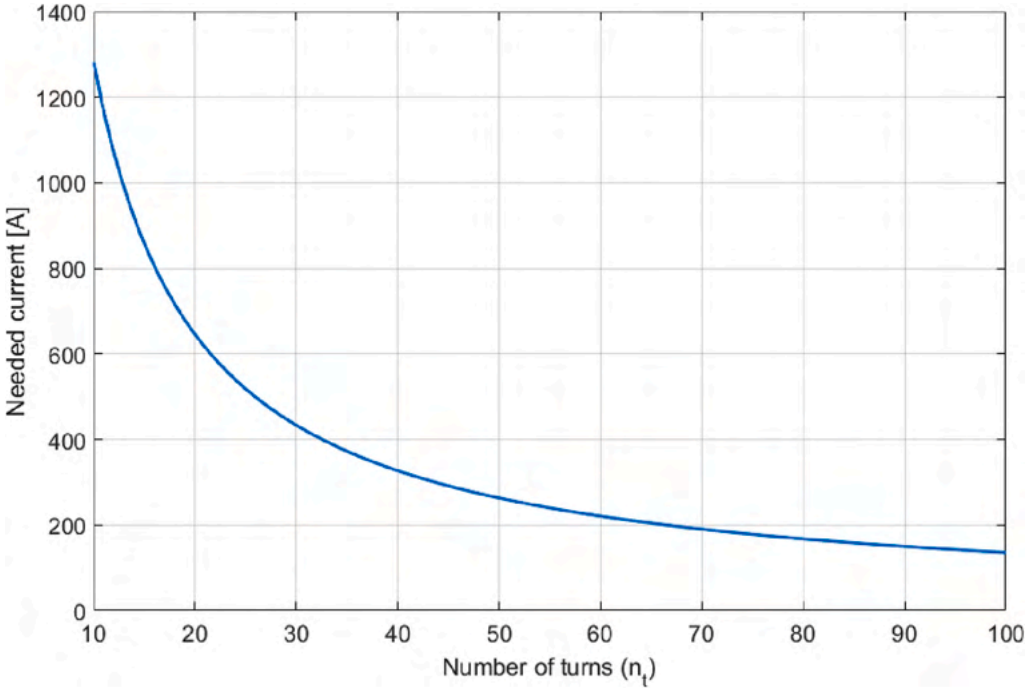

Fig. 7. Required current according to the number of turns (width = 5 mm, height = 5 mm, and thickness = 0.5 mm).

$$\sigma\left(\vec{E}_t + \vec{v} \times \vec{B}_t\right) = \sigma\{\left(E_r + v_{|03B8|}B_{i,z} + v_{|03B8|}B_{e,z}\right)\hat{r} + \left(E_z - v_{|03B8|}B_{i,r} - v_{|03B8|}B_{e,r}\right)\hat{z}\} \quad (12)$$

$$J_r = \sigma(E_r + v_\theta B_{i,z} + v_\theta B_{e,z}), J_\theta = 0, J_z = \sigma(E_z - v_\theta B_{i,r} - v_\theta B_{e,r}) \quad (13)$$

The helical-type MHD system generated fluid velocity in a narrow channel through Lorentz force, which only affects the fluid velocity in the θ direction, and is expressed using Eqs. (14)–(15) (also using Eq. (10)).

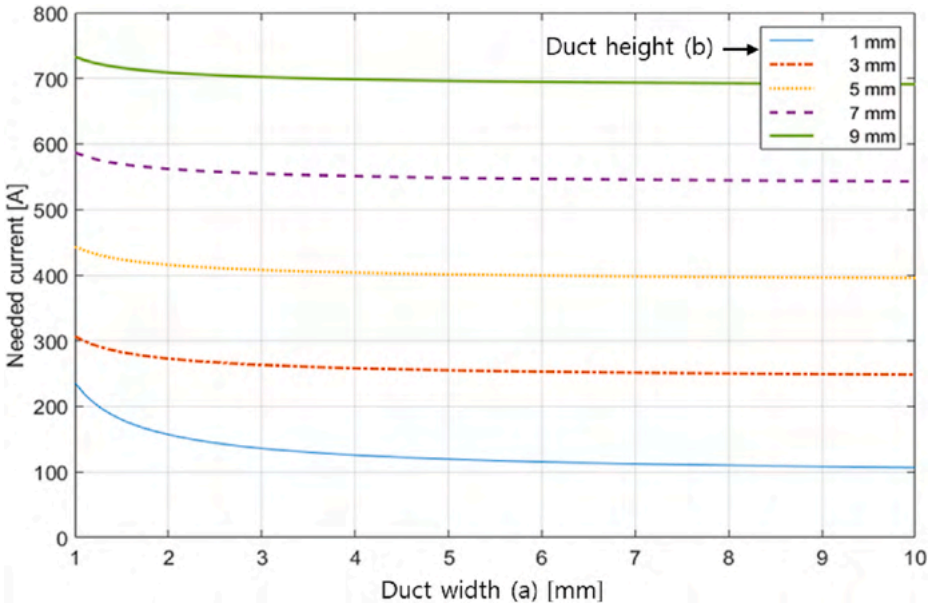

Fig. 8. Current required according to the height and width (thickness = 0.5 mm and number of turns = 30).

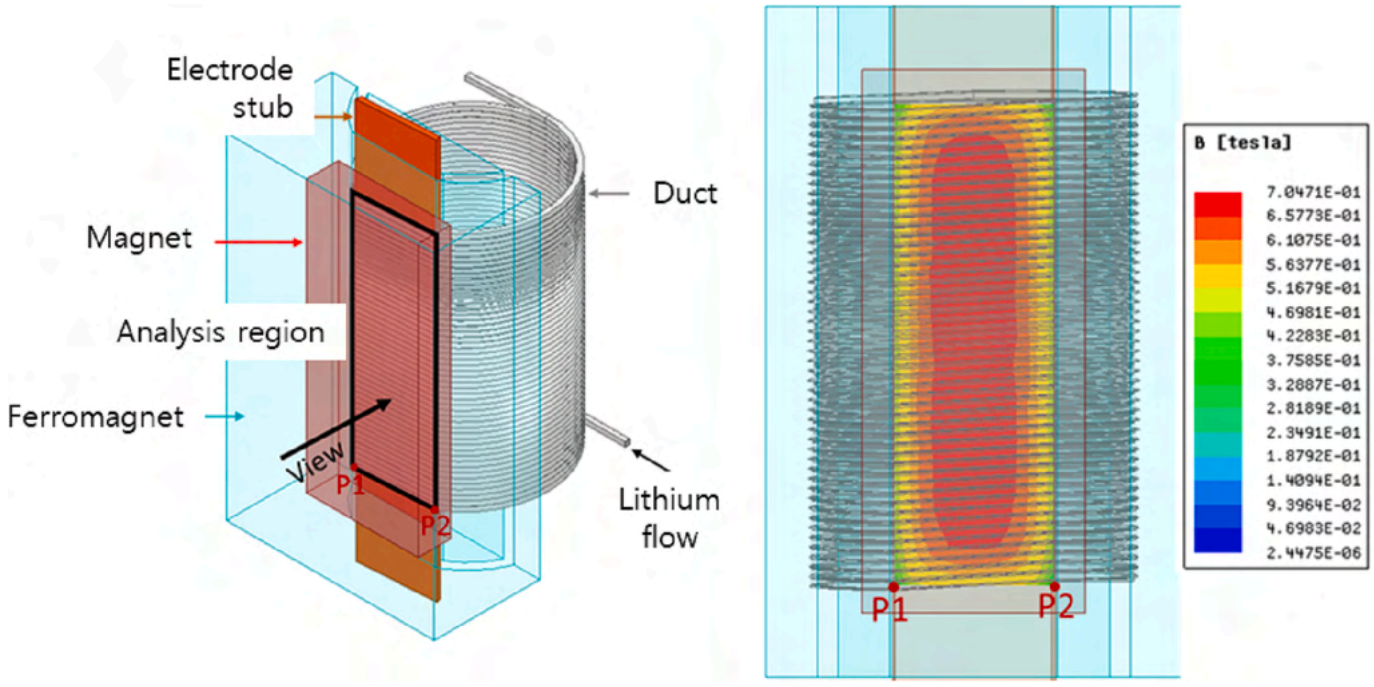

Fig. 9. Magnetic flux density distribution of the electromagnetic thruster.

$$\begin{aligned}\vec{f} = \vec{J} \times \vec{B} = &\{\sigma E_{[03B8]}(B_{i,r} + B_{e,r}) - \sigma(v_{[03B8]}B_{i,z} - v_{[03B8]}B_{e,z})(B_{i,[03B8]} + B_{e,[03B8]})\}\hat{z} \\ &+\{\sigma(E_z + v_{[03B8]}B_{i,r} + v_{[03B8]}B_{e,r})(B_{i,r} + B_{e,r}) - \sigma(v_{[03B8]}B_{i,z} + v_{[03B8]}B_{e,z})(B_{i,z} + B_{e,z})\}\hat{\theta}\ , \\ &+\{\sigma(E_z + v_{[03B8]}B_{i,r} + v_{[03B8]}B_{e,r})(B_{i,[03B8]} + B_{e,[03B8]}) - \sigma E_{[03B8]}(B_{i,z} + B_{e,z})\}\hat{r}\end{aligned} \tag{14}$$

$$f_\theta = \sigma(E_z + v_\theta B_{i,r} + v_\theta B_{e,r})(B_{i,r} + B_{e,r}) \tag{15}$$

For an MHD transportation system with a high Hartmann number owing to the magnetic field, the Navier–Stokes equation can be expressed using Eq. (16), which can be reduced to Eq. (17) for the steady-state incompressible flow of liquid metal, where the viscosity term can be ignored (Tillack and Morley, 1998). Accordingly, the Navier–Stokes equation's pressure gradient can be written as a number derived by multiplying the current density with the magnetic flux density.

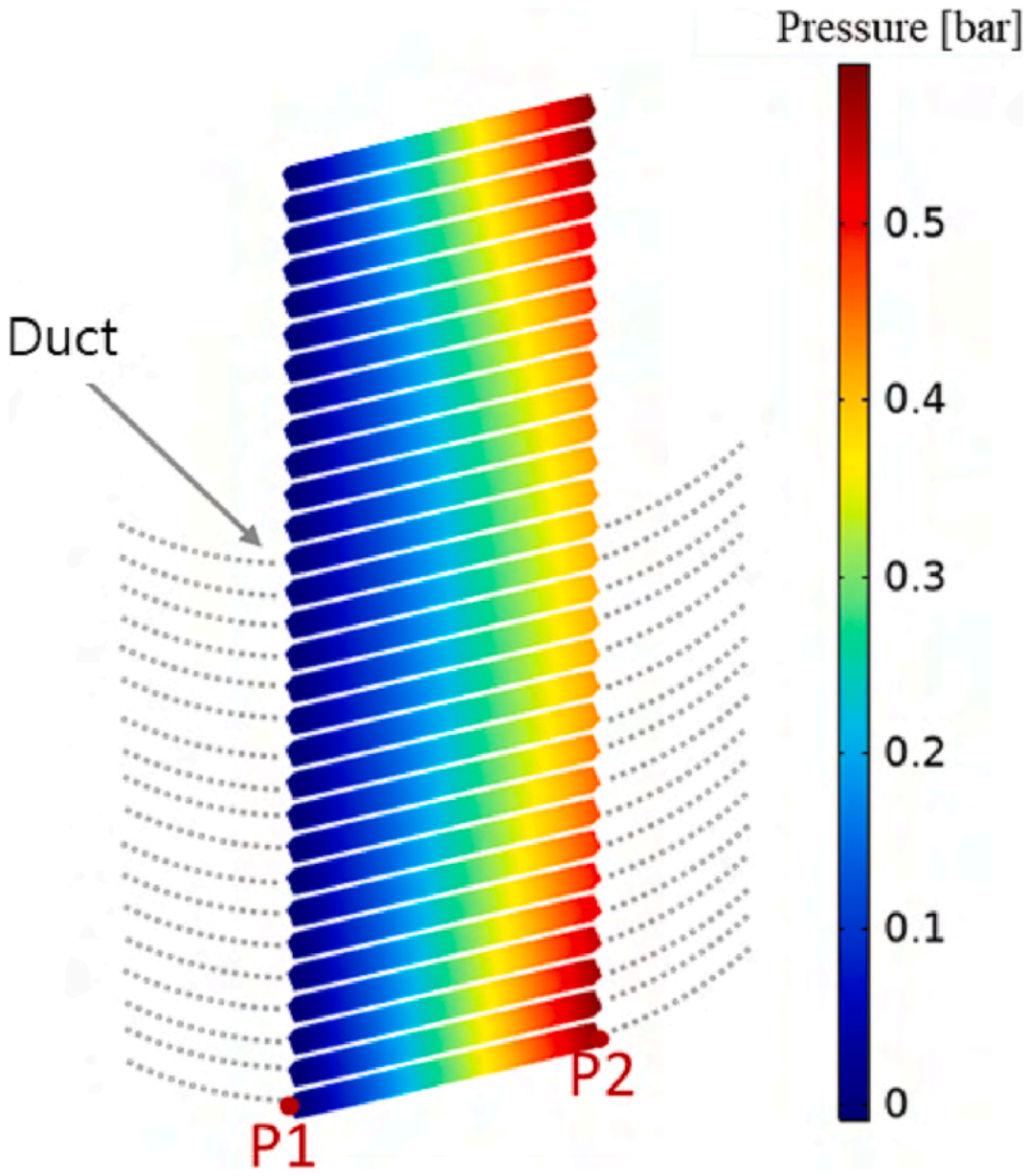

Fig. 10. Generated pressure of each pipe section of the electromagnetic thruster.

Table 1
Design variables of the electromagnetic thruster for FEM simulation.

Variable	Units	Values
Flow rate	[cm^3/s]	6
Developed pressure	[bar]	14.6
Temperature	[K]	473
Width and length of the flow channel (a,b)	[mm]	5
Thickness of the flow channel (t)	[mm]	0.5
Diameter of the flow channel (R)	[mm]	200
Length of electrode stub (c)	[mm]	50
Number of turns	–	30
Mean magnetic flux density	[T]	0.6
Input current	[A]	500
Weight	[kg]	21

$$\rho\left(\frac{\partial}{\partial t}+v\bullet\nabla\right)v=-\nabla p+\rho\nu\nabla^2 v+\overrightarrow{J}_t\times\overrightarrow{B} \tag{16}$$

$$\nabla p=\overrightarrow{J}_t\times\overrightarrow{B} \tag{17}$$

The hydraulic pressure loss between the flow inlet and outlet was computed using the Darcy–Weisbach formula expressed in Eq. (18).

$$\Delta p_h=f_d\rho L v_\theta^2/2D+K_B\rho L v_\theta^2/2, \tag{18}$$

$$\frac{1}{\sqrt{f_d}}=-1.8log_{10}\left[\frac{6.9}{Re}+\left(\frac{\varepsilon_s}{3.7D}\right)^{1.11}\right] \tag{19}$$

$$\mathrm{K_B}=(\mathrm{n}-1)(0.25\pi\mathrm{f_r r/d}+0.5\mathrm{K_1})+\mathrm{K_1} \tag{20}$$

By considering the hydraulic pressure, as expressed in Eq. (15), the pressure developed between the flow inlet and outlet (Eq. (21)) can be derived by combining Eqs. (15)–(20):

$$\Delta\mathrm{p}=4\int\{\sigma(E_z+v_\theta B_{i,r}+v_\theta B_{e,r})(B_{i,r}+B_{e,r})\}\mathrm{dV}/\pi\mathrm{d}^2-\mathrm{f_d}\rho\mathrm{L}v_\theta^2/2\mathrm{D}-\mathrm{K_B}\rho\mathrm{L}v_\theta^2/2 \tag{21}$$

The coupling between electromagnetic and fluid effects was calculated using COMSOL Multiphysics code simulation. The input variables

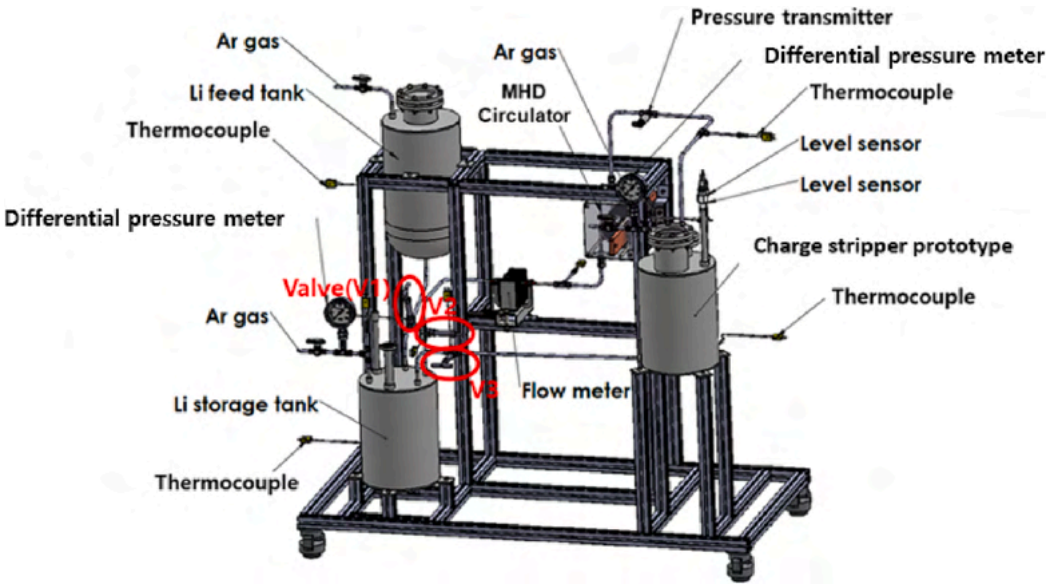

Fig. 11. Loop system for the electromagnetic thruster performance test.

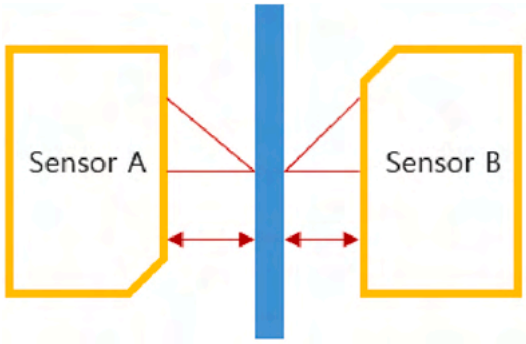

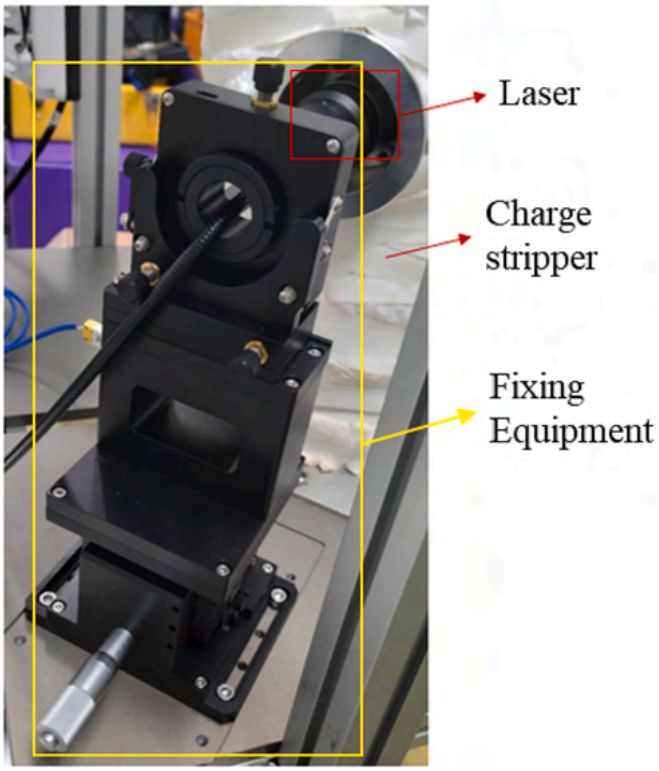

Fig. 12. Laser measurement method.

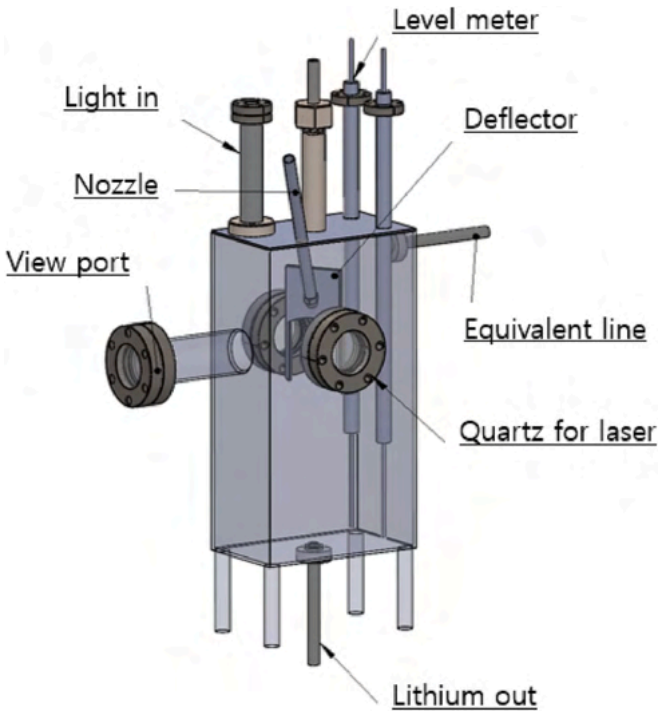

Fig. 13. Design of the charge stripper prototype.

included material properties, input current, and initial fluid dynamic conditions, and the output variables included the developed pressure and electromagnetic field distribution.

2.2. Equivalent circuit equation

Fig. 3 shows an illustration of the electric circuit methods for a helical-type MHD circulator. The force generated inside liquid lithium is affected by electromotive force (EMF) and the resistance of the thruster duct. To obtain the developed pressure in the liquid lithium of the thruster channel, equations for the helical-type MHD circulator were derived using Kirchhoff's and Ohm's laws (Nashine et al., 2007).

When an electric current flows through an electrode into an MHD

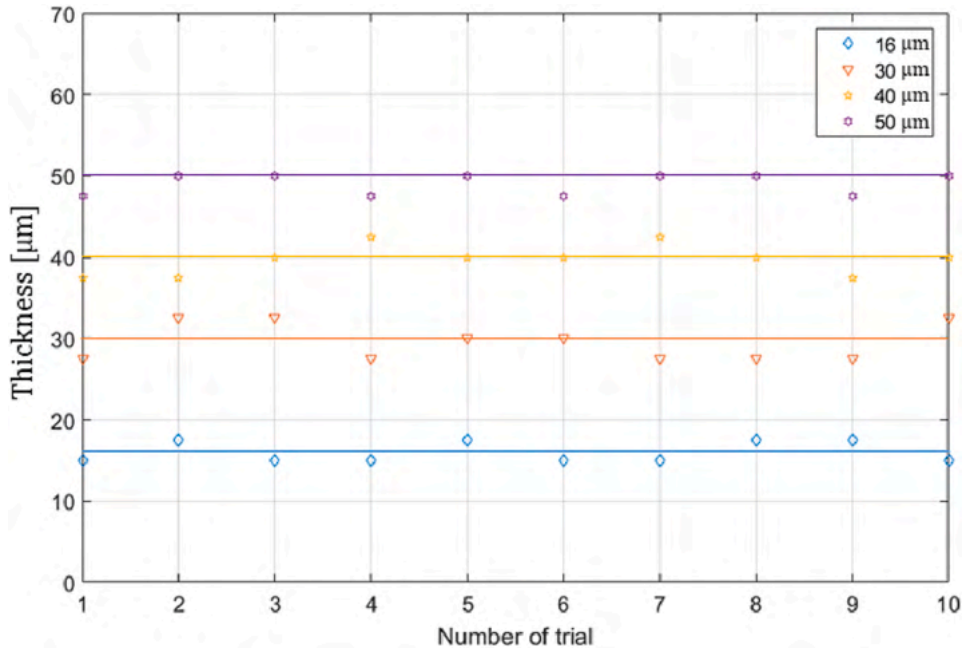

Fig. 14. Thickness calibration.

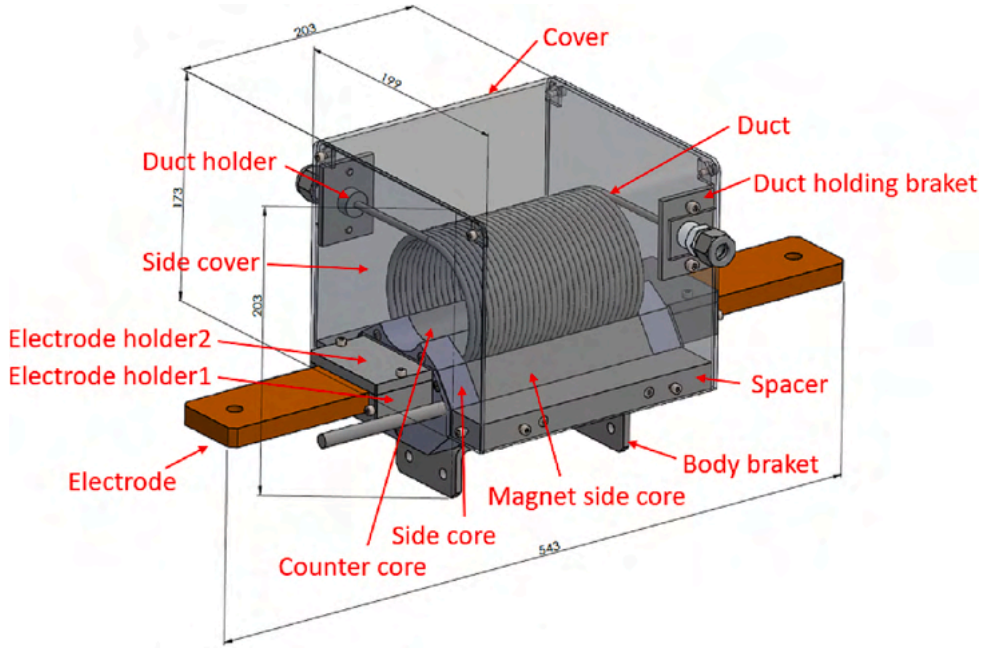

Fig. 15. Diagram of the electromagnetic thruster.

circulator, the current flows through the electrode.

Using Kirchhoff's law, the vertical component of the current flowing in the direction of the electrode stub and total input current can be expressed as:

$$i_{ver} = i_f + i_s \tag{22}$$

$$i_t = i_p + i_{ver} \tag{23}$$

The resistance in the direction vertical to the current flow can be expressed as:

$$\frac{1}{R_{ver}} = \frac{1}{R_f} + \frac{1}{R_s} \tag{24}$$

The voltage based on the current path can be determined using Ohm's law as:

$$R_o i_t + R_{ver} i_{ver} = R_o i_t + R_p i_p + E_p = V \tag{25}$$

According to the Lorentz principle, which follows an opposite trend to the generated force (voltage), the EMF interrupts the generated force (voltage) as follows:

$$E_p = BW_d v \tag{26}$$

The developed pressure was calculated by dividing the Lorentz force, which is the product of the magnetic flux density and current and width, by the flow area:

Fig. 16. Fabrication of the new electromagnetic thruster.

Table 2
Power supply specification.

	Value
Input voltage	380 V
Input current	30 A
Frequency	60 Hz
Output voltage	0–5 VDC
Output current	0–3000 A

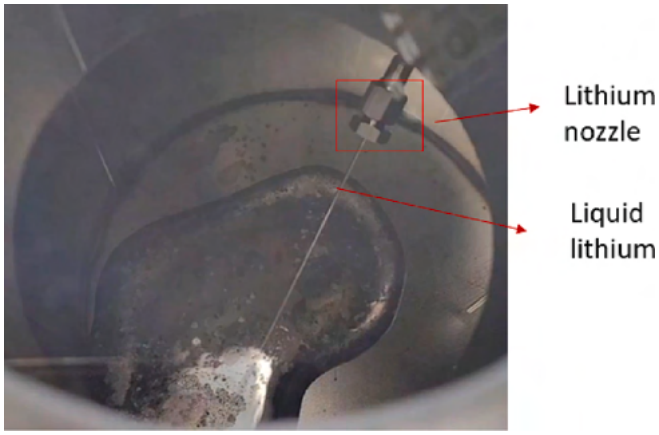

Fig. 17. Liquid lithium driving test.

Table 3
Results of the liquid lithium electromagnetic thruster driving test.

Current (A)	Developed pressure (bar)	Flow rate (cm^3/s)
100	1.63	2.87 (±0.02)
200	2.74	4.32 (±0.04)
300	4.01	5.12 (±0.06)
400	6.18	5.93 (±0.07)

$$\Delta P_L = \frac{B}{H_d} i_p \tag{27}$$

The current flowing in the liquid lithium was obtained by combining Eqs. (28)–(31) and eliminating the outer resistance and vertical current flow:

$$i_p = \frac{R_{ver} i_t - B w_d v}{R_p + R_{ver}} \tag{28}$$

Additionally, the hydraulic pressure drop was calculated using the Darcy–Weisbach formula:

$$\Delta P_h = \frac{f_d \rho L v^2 (W_d + H_d)}{4 W_d H_d} \tag{29}$$

The friction coefficient can be expressed as a function of the Reynolds number, hydraulic diameter, and roughness height (Haaland, 1983; Lee and Kim, 2017):

$$f_d = \frac{64}{Re} \tag{30}$$

$$\frac{1}{\sqrt{f_d}} = -1.8 \log_{10}\left[\frac{6.9}{Re} + \left(\frac{\varepsilon_s}{3.7D}\right)^{1.11}\right] \tag{31}$$

2.3. Helical-type electromagnetic thruster

The developed pressure was influenced by the multilayered duct geometry. Particularly, the permanent magnets and ferromagnetic materials in the θ direction did not dominantly affect the generated pressure. The geometry of the magnets and ducts was changed for maintenance (Fig. 4). The total weight of the thruster was reduced from 340 to 21 kg, to enable usability and maintenance.

Fig. 5 shows the shape of the MHD electromagnetic thruster used for the COMSOL simulation, in which the width, height, thickness, length, and number of turns were set as variables. The Lorentz force generated increased as the magnetic flux density increased, resulting in the reduction of the required current. In addition, a ferromagnetic material, namely, ferromagnetic steel, was introduced to increase the magnetic flux density. Fig. 6 shows the magnetic flux density according to the thickness of the ferromagnetic material. The thickness of ferromagnetic steel was set to 20 mm by considering maintenance issues—a further increase in the thickness beyond 20 mm increased the weight, making duct maintenance difficult.

As the number of turns in the duct increased, less current was required because the number of revolutions was equal to the number of times the Lorentz force was applied. Fig. 7 shows the relationship between the required current and number of turns. By considering the duct productivity, the number of rotations was determined as 30.

Fig. 8 shows the variation in the geometry of the MHD electromagnetic thruster. Increasing the duct width reduced the required current owing to the reduced hydraulic friction losses, whereas increasing the duct height increased the required current. This, a small duct height was utilized to prevent the clogging of the pipe with lithium oxide and to prevent the possibility of filling the thruster duct with steam, which interferes with the current flow. In this study, a 5-mm-height-long rectangular duct was adopted.

When a ferromagnetic material was used in the magnet, the mean magnetic flux density of the MHD electromagnetic thruster was 0.6 T (Fig. 9). The ferromagnetic material created a maximum magnetic flux density at the center. When an input current of 500 A was passed through the electromagnetic thruster, as shown in Fig. 10, a pressure of 14.6 bar is generated. Each duct generated a pressure of approximately 0.5 bar.

Table 1 lists the design parameters of the new MHD electromagnetic thruster (Haaland, 1983). The graph was optimized at approximately 6 cc/s. The total weight of the redesigned model was reduced to 6% of that of the existing design model. In addition, the input current was reduced

from 872 to 500 A, which was decreased to 57%, and the developed pressure was 40 % higher than that of the conventional units, where it increased from 10.5 to 14.6 bar (Lee and Kim, 2017). The light weight of the redesigned thruster will enable its maintenance, and the newly designed MHD electromagnetic thruster could generate high-specification driving pressure at a lower current. In addition, the driving pressure of the new lightweight MHD electromagnetic thruster was 2.4 times greater than that of the existing thruster at the same input current (Lee and Kim, 2017).

2.4. MHD electromagnetic thruster experimental setup (with thickness measurement)

Fig. 11 shows the lithium-circulating system and its main components, namely, the lithium feed tank, lithium storage tank, MHD electromagnetic thruster, and charge stripper prototype. The lithium feed tank supplies lithium, and the lithium storage tank stores lithium when the system is not functional. The electromagnetic thruster installed in the circulation system was driven to drain liquid lithium from a thin nozzle within the charge stripper prototype.

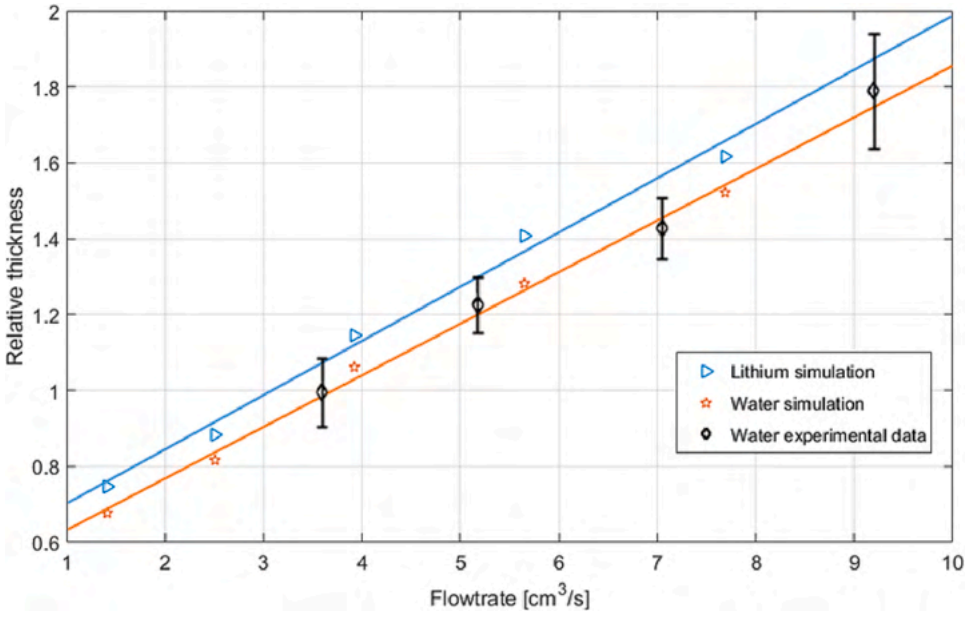

Fig. 18. Finite element method (FEM) simulation analysis results of the water and lithium thickness.

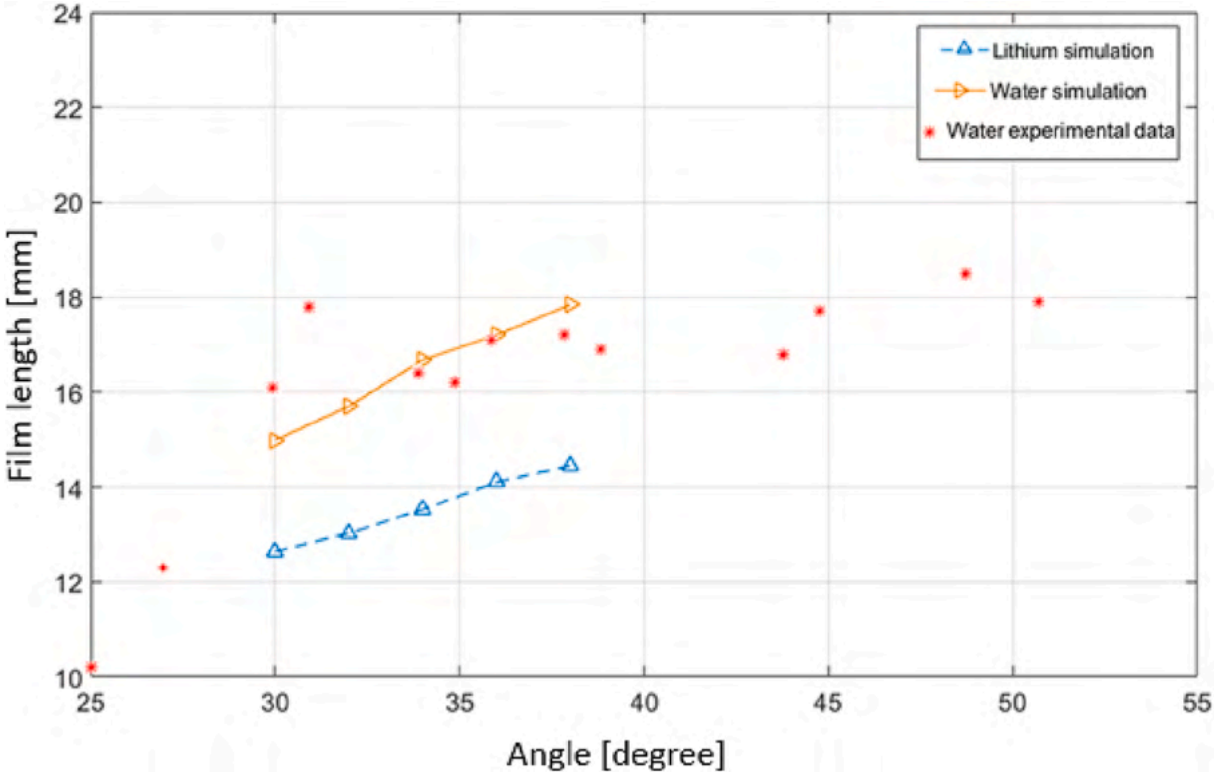

Fig. 19. Change in the film length as a function of the angle.

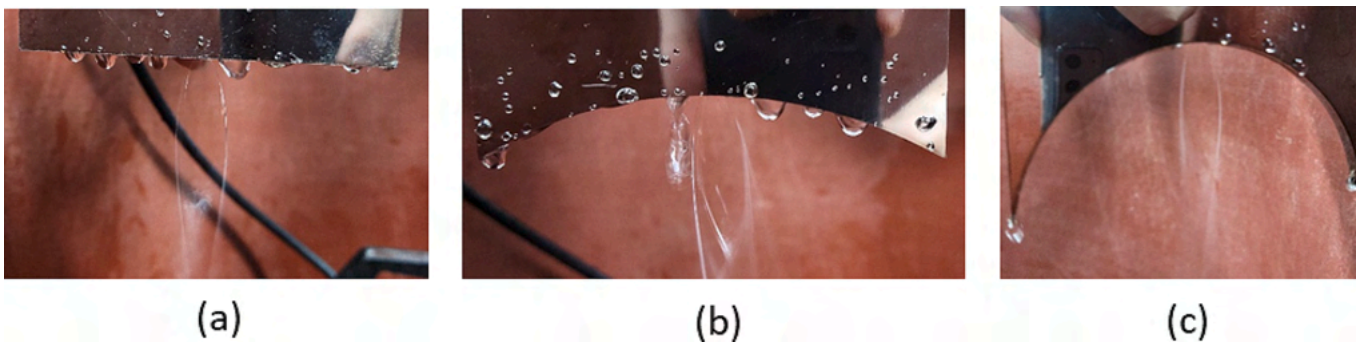

Fig. 20. Deflector experiment: (a) flat, (b) R100, and (c) R50.

2.5. Aluminum foil-based testing of the performance of the laser measurement system for the thickness measurement of the liquid lithium film

Existing technologies measure the thickness of lithium thin films using electron guns, but electron guns emit electron beams, which can cause radiation exposure problems; thus, radiation permission procedures are required for their use (Halfon et al., 2014). Therefore, this study employed a laser measurement system (as shown in Fig. 12) to reduce unnecessary procedures and implement safe experimental methods. This system exhibits an alignment function, and the different wavelengths ejected from the laser were transmitted to the computer. The alignment was performed until the two lasers exhibited the same diffracted wavelengths location. Accordingly, the distance between the two devices can be determined using the reference specimen. After alignment, the distance between the two devices was determined using the reference specimen. Two laser devices (Model CL-3000) were installed, and the thickness of the lithium thin film was measured by calculating the change in the laser transmission time with a change in the distance between the liquid lithium thin film and the laser device. In terms of specification, the resolution of the laser device was 2.5 μm and the measurable distance of the laser device was 120 to 160 mm. As only a short distance can be measured, the shape of the charge stripper prototype was changed, as shown in Fig. 13.

The containment unit of the charge stripper prototype contained a viewport for observing the state of the liquid lithium film. The deflector and nozzle influenced the formation of the liquid lithium film, and the level meter measured the flow rate of the electromagnetic thruster. The equivalent line functioned to equalize the pressure of the lithium film and storage tank, and the quartz view port was used to visually observe the measurement performed by the laser device. Thickness calibration verification was performed (Fig. 14) using 16-, 30-, 40-, and 50-μm aluminum foils, whose thicknesses were determined using the installed charge stripper prototype. Fig. 14 shows that the measurement errors at thicknesses of 16, 30, 40, and 50 μm were ±1.5, ±2.5, ±2.5, and ±2.5 μm, respectively, while the deviation interval of 2.5 μm satisfied the resolution of the laser thickness measurement system. In addition, the standard deviations at thicknesses of 16, 30, 40, and 50 μm were 1.29, 2.29, 1.84, and 1.29 μm, respectively, while the deviation interval of 2.5 μm satisfied the resolution of the laser thickness measurement system.

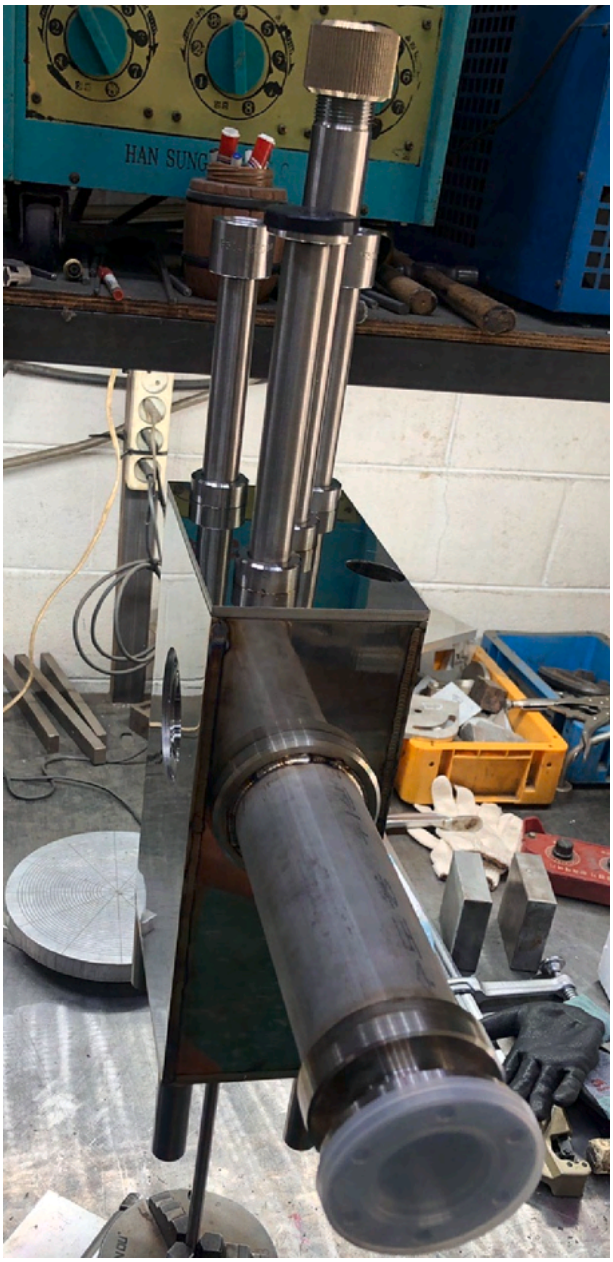

Fig. 21. Fabricated charge stripper prototype.

3. Results and discussion

3.1. Electromagnetic thruster

Fig. 15 shows a schematic representation of the newly redesigned MHD electromagnetic thruster consisting of electrodes for supplying current, brackets for fixing, ducts, magnets, and a core. As copper

electrodes cannot be employed for prolonged periods because they undergo rapid oxidation at high temperatures, SUS316-based electrodes were used in this study.

The fabrication process of the new MHD electromagnetic thruster is shown in Fig. 16. The reduction in the weight of the thruster from 340 to 21 kg for easy maintenance facilitated the removal of the magnet core. Consequently, the flow path structure of the MHD electromagnetic thruster can be easily replaced in the case of an accident. The specifications of the power supply used in the MHD electromagnetic thruster are shown in the Table 2.

The MHD electromagnetic thruster was successfully driven via a driving process (Fig. 17). To obtain precise measurement values, several differential pressure gauges and flow meters were installed in the loop system. The developed pressure and flow rate measured as a function of the current are presented in Table 3. Table 3 indicates that the developed pressure at 500 A is 8.95 bar, which is 0.62 times smaller than the simulation value (14.6 bar). This difference was attributed to the reduction in the magnetic flux density at a high temperature and fringing current from actual soldering.

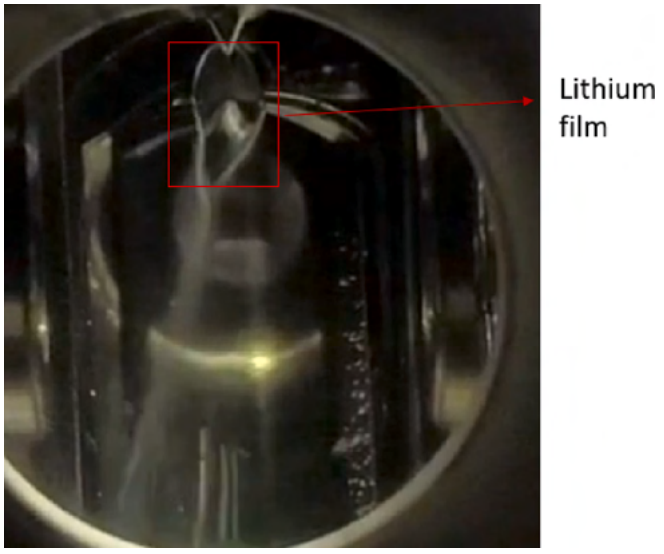

Fig. 22. Liquid lithium film formation experiment.

In this study, FEM simulations were performed to verify the water test results and the trend of the change in the thickness with a change in the flow rate, and the results are shown in Fig. 18. The surface tension of liquid lithium is greater than that of water, and the difference in the Reynolds number of the two is approximately 1.2. Water and lithium have similar results owing to their similar Reynolds number, which is a major factor in film formation. The simulation results revealed that the thickness of lithium was 1.1 times higher than that of water. The results of the water simulation were consistent with the water experimental data.

The nozzle angle was analyzed through the water experiments. As shown in Fig. 19, the length of the resulting lithium film was stable between 30 and 38°, beyond which the length values did not exhibit a linear trend, so the average nozzle angle was determined to be 34°. To achieve the 22-μm thickness of the lithium film, a nozzle with a minimum thickness of 0.7 mm was determined as ideal.

The deflector was designed and constructed to determine the characteristics of the liquid thin film with a change in the shape of the deflector. A change in the radius of the deflector (50 and 100 mm) exerted no significant impact on the shape of the film (Fig. 20(b) and (c)). However, the curvature of the deflector enabled the coalescence of the droplets. As the curvature increased, the deflector radius was set to 50 mm to decrease the number of water droplets that can interfere with lithium film formation. The geometry of the deflector had no significant effect on the film thickness.

Fig. 21 shows the fabricated charge stripper prototype.

3.2. Experimental analysis of the liquid lithium film thickness

Fig. 22 shows the successful formation of a liquid lithium film. The liquid lithium sprayed through the nozzle collided with the deflector to form a thin film. The thickness of the thin film was measured using a laser thickness gauge. The thickness of the thin film based on the flow rate is shown in Fig. 23. It could be experimentally demonstrated that the flow rate and thickness of the lithium thin film increased as the input current increased, and a current of 107 A was required to achieve the thickness. Additionally, the standard deviation at 107 A was 4.3 μm. The laser measuring device measures the thickness at the time the laser is reflected. The shape of the lithium film became inflated owing to splashing liquid, and the bouncing off of lithium increased with an increase in the input current, resulting in an unstable shape. As shown in Fig. 24, a liquid lithium film thickness of 1.13 mg/cm^2 is required to

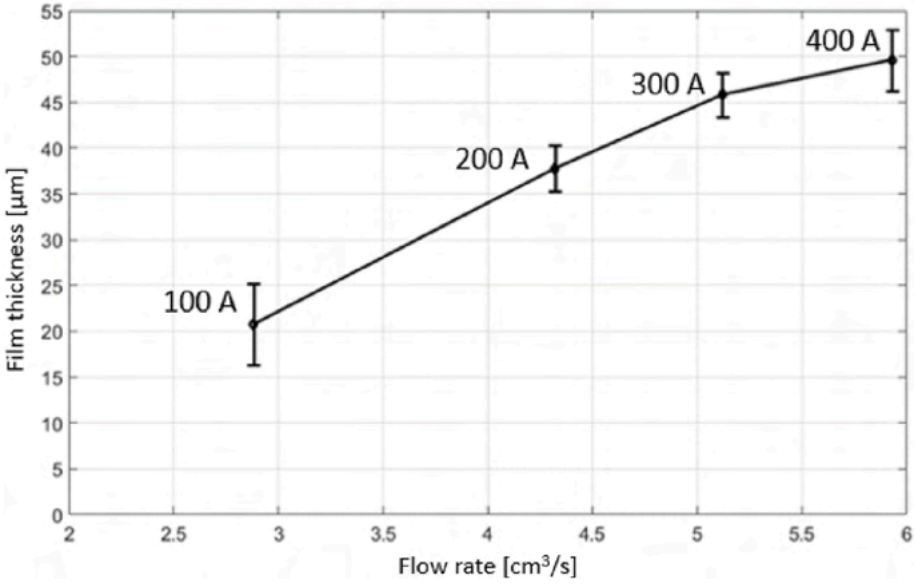

Fig. 23. Liquid lithium film thickness according to the flow rate.

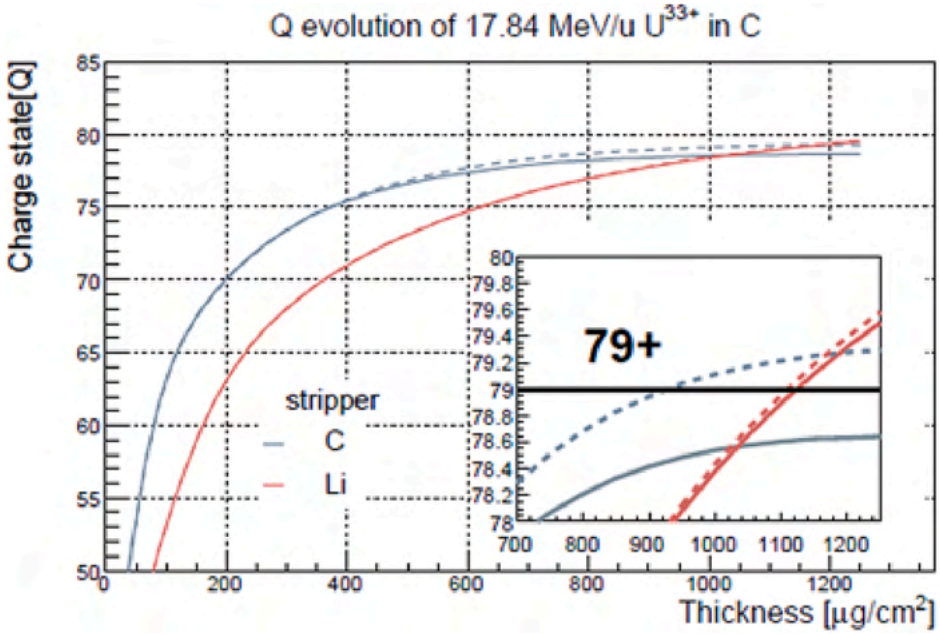

Fig. 24. Charge state according to thin film thickness.

achieve the 79 $^{+}$ charge state of uranium. Particularly, according to the graph (Fig. 24), to achieve a charge state value of 78^{+}–80^{+}, the thickness of the lithium film must be within 800 to 1400 (i.e., 15 to 27 μm when converted). According to Fig. 23, the 79^{+} state ($78.x^{+}$ state–$79.x^{+}$ state) can be achieved at a thickness of 16–25 μm.

4. Conclusions

This study optimized a prototype of a lithium charge stripper used in RAON for the removal of uranium charges to ensure easy maintenance and significantly reduce its weight. The thickness of the thin film with a change in current was measured using a new laser measurement method. Compared to traditional electron gun methods, licensing procedures can be omitted using this method, significantly reducing usage time and eliminating the need to consider radiation exposure issues.

The input current of the newly-constructed electromagnetic thruster and its weight were reduced to 57% and 6%, respectively, which enables easy maintenance. The results revealed that the ideal nozzle diameter and angle that ensured stability and satisfied the lithium film thickness (22 μm) were 0.7 mm and 34°, respectively. Additionally, the deflector was manufactured with a curvature that minimized the contamination problem of lithium droplets. The results confirmed that the flow rate and liquid lithium film thickness increased as the input current increased. It was shown the liquid lithium thin film thickness of 22 μm could be achieved at an input current of 107 A.

This research provides experimental evidence for the fabrication of an MHD electromagnetic thruster-based charge stripper prototype. This optimized charge stripper prototype can be used to fabricate liquid lithium films for increasing the charge state of heavy-ion beams passing through it to obtain an energy of 200 MeV/u.

CRediT authorship contribution statement

Tae Uk Kang: Software, Formal analysis, Writing – original draft. **Geunhyeong Lee:** Conceptualization, Methodology. **Hee Reyoung Kim:** Supervision, Project administration.

Declaration of Competing Interest

The authors declare the following financial interests/personal relationships which may be considered as potential competing interests: Hee Reyoung Kim reports financial support was provided by Korea Institute of Energy Technology Evaluation and Planning.

Data availability

Data will be made available on request.

Acknowledgment

This work was supported by the Rare Isotope Science Project of the Institute for Basic Science funded by Ministry of Science and ICT and NRF of Republic of Korea (2013M7A1A1075764), the Korea Institute of Energy Technology Evaluation and Planning, and the Ministry of Trade, Industry & Energy (MOTIE) of the Republic of Korea (grant no. 20214000000410).

References

Haaland, S.E., 1983. Simple and explicit formulas for the friction factor in turbulent pipe flow. J. Fluids Eng. 105 (1), 89–90.
Halfon, S., Paul, M., Arenshtam, A., Berkovits, D., Cohen, D., Eliyahu, I., Kijel, D., Mardor, I., Silverman, I., 2014. High-power electron beam tests of a liquid-lithium target and characterization study of 7Li (p, n) near-threshold neutrons for accelerator-based boron neutron capture therapy. Appl. Radiat. Isot. 88, 238–242.
Lee, G.H., Kim, H.R., 2017. Numerical investigation and comparison of the rectangular, cylindrical, and helical-type DC electromagnetic pumps. Magnetohydrodynamics 53 (2), 429–438.
Lee, G.H., Kim, H.R., 2018. Magnetohydrodynamics approach for active decay heat removal system in future generation IV reactor. Int. J. Energy Res. 42 (10), 3266–3278.
Momozaki, Y., Nolen, J., Reed, C., Novick, V., Specht, J., 2009. Development of a liquid lithium thin film for use as a heavy ion beam stripper. J. Instrum. 4 (04), P04005.
Nashine, B.K., Dash, S.K., Gurumurthy, K., Kale, U., Sharma, V.D., Prabhakar, R., Rajan, M., Vaidyanathan, G., 2007. Performance testing of indigenously developed DC conduction pump for sodium cooled fast reactor. Indian J. Eng Mater. Sci. 14, 209–214.
Rare Isotope Science Project (2012) *Baseline design summary*.
Reed, C.B., Nolen, J.A., Specht, J.R., Novick, V.J., 2016. Engineering and safety issues of lithium targets and film strippers. Proceedings of the Sixth International Meeting on Nuclear Applications of Accelerator Technology.
Song, J., 2016. Study of the interaction of charged ions with matter-development of charge stripper and IF production target at RISP. Seoul National University. Doctoral dissertation.
Tillack, M.S., Morley, N.B., 1998. Magnetohydrodynamics. McGraw-Hill.